Dynamic dephasing of magnetization precession in arrays of thin magnetic elements

Anjan Barman* and Saswati Barman
Department of Physics, Indian Institute of Technology Delhi, Hauz Khas, New Delhi 110016, India
(Received 20 October 2008; revised manuscript received 11 February 2009; published 15 April 2009)

We present a systematic micromagnetic simulation to demonstrate how the static and dynamic behaviors of single nanomagnets are modified in an array. We examine the precessional frequency and damping as a function of the width to separation (w/s) ratio in arrays of square and circular magnetic elements and compare it with the single nanomagnet dynamics. Both frequency and damping are significantly modified by the interelement interaction. The precessional frequency shows a general trend of increase with w/s ratio due to the increase in the dipolar magnetic field in the array and split into multiple modes when the w/s ratio becomes greater than 1. The damping of precession increases with increase in w/s ratio, i.e., with decrease in the separation between the elements. The increase in damping is found to be due to the mutual dephasing of precession of elements in an array. For larger square nanomagnets, (width=150 nm, thickness=50 nm), where the single nanomagnet dynamics is inherently nonuniform, the effect of the array only increases the incoherence in the precession. For larger circular nanomagnets, (width=150 nm, thickness=50 nm), where the single nanomagnet shows slow vortex core oscillation, the array modifies the dynamics into incoherent spin-wave dynamics whose coherence increases with the increase in w/s ratio. Analysis of static and dynamic magnetic images reveals that the dynamics is strongly dependent on the static magnetization in the arrays. The results presented here show that the dynamics of arrays of nanomagnets is significantly or entirely different from that of individual elements, and hence measurements from arrays may not be considered as the single nanomagnet dynamics. We also evaluate the role of dynamic dephasing in the increased damping coefficient.

DOI: 10.1103/PhysRevB.79.144415 PACS number(s): 75.40.Gb, 75.30.Ds, 75.75.+a

I. INTRODUCTION

Nanomagnets form the building blocks for data storage devices such as patterned magnetic media and magnetic random access memory.[1] New effects such as spin transfer torque induced magnetization reversal also show exciting promises.[2,3] Magnetic nanoparticles on the other hand play an important role in targeted drug delivery,[4] magnetic resonance imaging,[5] and magnetic sensors.[6] Numerous new physics and phenomena are being proposed based on nanomagnets.[7,8] For device applications, regular arrays of nanomagnets such as those used in patterned magnetic media are very important. However, in a closely packed array the role of dipolar interaction cannot be neglected. Efforts have been made into understanding the magnetic switching field distribution in the quasistatic magnetization reversal;[9,10] while precessional dynamics from arrays of nanomagnets are only beginning to be explored.[11–15]

Nondestructive methods of detection of magnetic properties especially from confined magnetic structures and surfaces of thin films and the development of magneto-optical data storage have made the magneto-optical detection methods [magneto-optic Kerr effect (MOKE)] very popular.[16–19] The static[20] and time-resolved[13–15] MOKE investigations of nanomagnets have made use of array measurements due to the enhancement of the total MOKE signal from a large number of elements in an array falling within the area of a diffraction limited laser spot (~ 1 μm). However, in doing so the intrinsic properties of the individual nanomagnet are not measured and instead a collective response is detected. While in quasistatic measurements the ensemble effect shows up in the switching field distribution,[9,10] the dynamics is even more complicated since precession frequency, damping, and overall amplitude and trajectory of the magnetization are affected by the ensemble effect.[13–15] If precessional switching has to be introduced in the read-write processes of magnetic data storage, the above issues must be addressed and understood and finally eliminated. Only a few studies of magnetization dynamics in nanomagnet arrays have been reported so far.[11–15] Very recently time-resolved dynamics of single nanomagnets[21–23] has started to be explored and the existing reports strongly suggest the importance of single element measurements for understanding the intrinsic dynamics. Particularly Ref. 21 has clearly pointed out the differences in the precessional dynamics between single elements and arrays.

In this work we present a systematic micromagnetic simulation study of arrays of square and circular thin magnetic elements. We examined the precessional frequency and damping as a function of the width to separation (w/s) ratio in arrays and compared it with single nanomagnet dynamics. We have considered two different shapes, square and circle, to demonstrate the effect of self-magnetostatic energy and the symmetry of the dipolar field on the dynamics. We have also considered nanomagnets of different dimensions to investigate the effect of the magnetic ground-state configuration on the collective dynamics. The single nanomagnet and array configurations made of 60 nm width and 5 nm thickness are studied first since the individual elements of this dimension show nearly single domain magnetic ground states. For larger elements (width=150 nm, thickness =50 nm) the ground state is quasiuniform, leading to a largely nonuniform precession in the individual elements. The nonuniformity in the precession of individual elements makes the dynamics of the arrays very rich. A common feature of all cases is a modification of the frequency spectra in the arrays and an increase in the apparent damping of pre-

cession. In the case of larger circular elements apparently an opposite behavior is observed where the increased packing density leads to an increase in the coherence of precession. We analyze all these observations with the aid of simulated static and time-resolved magnetic images. In addition to the intrinsic damping coefficient the relaxation of the dynamics in arrays of submicron elements is affected by two extrinsic effects, the nonuniform demagnetizing field within individual elements and the interelement dipolar interaction. In this paper we isolate, quantify, and understand the role of the above two effects in the damping of the collective dynamics in arrays.

II. METHOD

We have studied arrays of square and circular $Ni_{81}Fe_{19}$ (permalloy) elements with "width × thickness" of individual elements as 60 nm × 5 nm, 150 nm × 50 nm, and 150 nm × 10 nm. The arrays were made of 7 × 7 elements, since we found this is the minimum number of elements required to correctly include the effect of long-range magnetostatic interaction in a large array. This is supported by earlier reports of micromagnetic simulations on arrays.[24] Time-dependent micromagnetic simulations were performed by solving the Landau-Lifshitz-Gilbert (LLG) equation[25] using the public domain software called Object Oriented Micromagnetic Framework (OOMMF) from the NIST website.[26] Calculations were performed by dividing the samples into a two-dimensional array of cells with dimensions of 5 nm × 5 nm × t for square elements and 3 nm × 3 nm × t for circular elements, where t is the thickness of the sample. Further simulations were performed on square elements with 3 nm × 3 nm × t and 5 nm × 5 nm × 2 nm cells but no significant changes were observed in the static and dynamic magnetic behaviors. However, for single circular elements and arrays of circular elements with 150 nm width and 50 nm thickness a marked change in the static and dynamic magnetization is observed for lateral cell size below 5 nm. In addition, to minimize the possible discretization errors in building a cylindrical structure with cuboidal cells in the finite difference analysis method as used in the OOMMF simulations, we have used cells with dimension 3 nm × 3 nm × t for all circular elements presented here. The linear dimensions of the cells are less or equal to the exchange length, which is defined as $\sqrt{(A/2\pi M^2)}$ where A is the exchange constant and M is the magnetization, respectively, and has a value of about 5 nm in permalloy. Further discussions regarding the dependence of micromagnetic simulation results on cell size may be found elsewhere.[27,28] The change in relative energy error as cell size reduces well below the exchange length is generally not significant compared to the increase in the required computation time. Details on doing micromagnetic simulations with OOMMF may be found elsewhere.[29,30] The finite thickness of the film affects the result through the demagnetizing field, which is evident from different magnetization configurations of elements with same width but different thickness values as shown later in this paper.

The static magnetic configuration was obtained by first applying a large enough bias field to fully magnetize the sample and allowing the magnetization to relax for 12 ns. The applied field was then reduced to the bias field values and the magnetization was further allowed to relax for another 12 ns. During this process α was set at 0.5 so that the precession dies down quickly and the magnetization fully relaxes within 12 ns. The simulations assume typical material parameters for permalloy, $4\pi M_S = 10.8$ kOe, $A = 1.3 \times 10^{-6}$ erg/cm, $H_K = 0$, and $g = 2.2$. The pulsed magnetic field $\mathbf{h}(t)$, with rise time of 50 ps and peak amplitude of 30 Oe, was applied to the sample in the configurations as shown in Figs. 1(a) and 1(b) and the dynamic magnetization and magnetic fields averaged over the entire sample volume and images of the same were saved for a total duration of 4 ns at intervals of 10 ps. A unique damping parameter of 0.008 for permalloy was assumed in the dynamic simulations.

III. RESULTS AND DISCUSSIONS

We have investigated the dependence of the static and time-resolved magnetization on the cell size used in the simulations and Figs. 1(c)–1(e) show some examples of those results. Figure 1(c) shows the static magnetic configuration and Fig. 1(d) shows the time-resolved magnetization and corresponding fast Fourier transform (FFT) spectra of a circular element with 60 nm width and 5 nm thickness when the simulation is performed with variable cell sizes of 5, 3, and 2 nm. No appreciable changes either in the static magnetic configuration or in the frequency and damping of precession of magnetization are observed with the variation in cell size. Further, we have simulated the static magnetic configuration of a square element with 150 nm width and 50 nm thickness with cell size of 5 nm × 5 nm × 2 nm as shown in Fig. 1(e). The static magnetization configuration is found to be independent of discretization along the thickness of the element, which justifies the choice of cell size used in the simulations presented here. Figures 2(a) and 2(b) show the time-dependent magnetization (M_z) and the corresponding FFT spectra for single elements and arrays of elements of square and circular shapes of 60 nm width and 5 nm thickness, respectively. A bias field of $H_{\text{bias}} = 500$ Oe was applied to ensure saturated static magnetization for the single element. The edges parallel to the bias field show the sign of relatively small demagnetized areas for these samples. The time-resolved magnetization and the corresponding FFT spectra show a uniform precession mode for the single element. This is a desired situation, which would allow us to isolate the effect of the dipolar interaction between the elements in an array from the dynamics of the single element. The time-dependent magnetization and the FFT spectra from the arrays with increased width to separation (w/s) ratio show two effects. First, the decay time of precession reduces steeply while retaining the single precession mode down to $w/s = 1$. However, for $w/s > 1$, beating appears in the time-resolved data revealing a number of modes in the FFT spectra for w/s ratio up to 3. We find the decay time τ by fitting the time-dependent magnetization with a damped sine function with single frequency

$$M(t) = M(0)e^{-t/\tau}\sin(\omega t - \phi). \quad (1)$$

Consequently the effective damping coefficient α_{eff} in the LLG equation is extracted from $\tau = \frac{1}{\omega\alpha_{\text{eff}}}$; ω is the angular

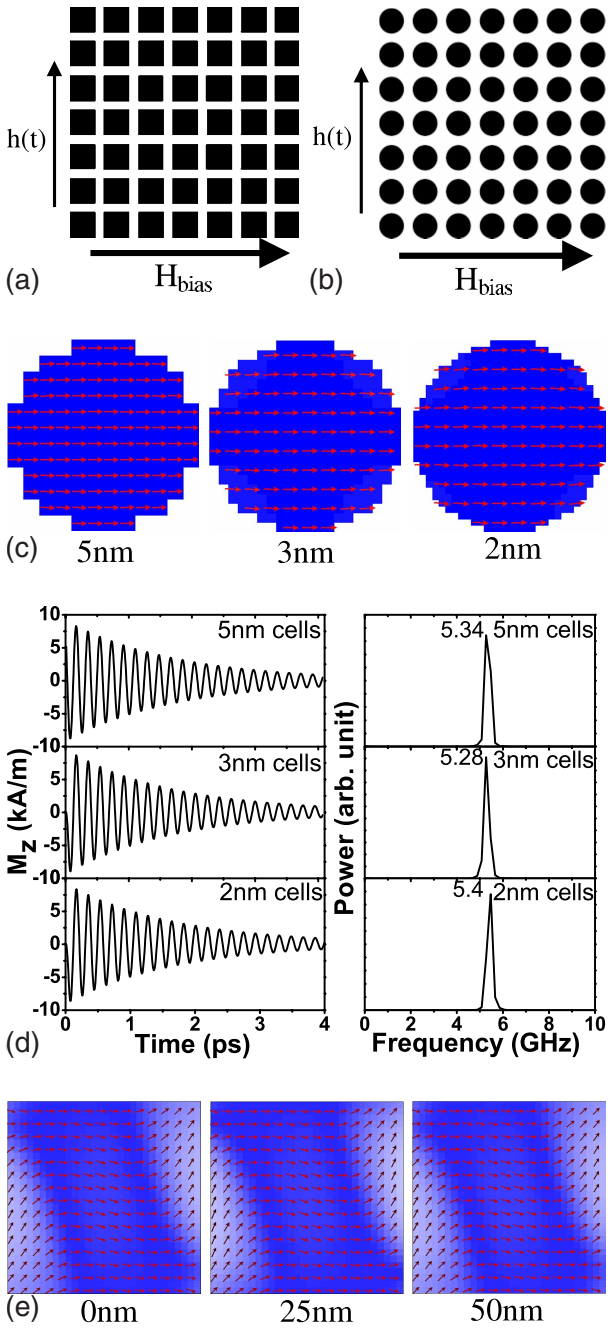

FIG. 1. (Color online) (a) Geometry of simulation of the time-resolved dynamics for single $Ni_{81}Fe_{19}$ elements and arrays of $Ni_{81}Fe_{19}$ elements of (a) square shape and (b) circular shape. (c) The static magnetic configuration and (d) time-dependent magnetization (left panel) with corresponding FFT spectra (right panel) are shown for a circular element with 60 nm width and 5 nm thickness for three different cell sizes (5 nm $\times$ 5 nm $\times$ 5 nm, 3 nm $\times$ 3 nm $\times$ 5 nm and 2 nm $\times$ 2 nm $\times$ 5 nm) used in the OOMMF simulations. A bias field H_{bias}=500 Oe is applied in the geometry as shown in Fig. 1(b) for the above simulations. (e) The static magnetic configuration of a square $Ni_{81}Fe_{19}$ element with a bias field H_{bias}=500 Oe applied in the geometry as shown in Fig. 1(a) is shown. The simulation was performed with cell size of 5 nm $\times$ 5 nm $\times$ 2 nm and the in-plane magnetizations at three different heights of the sample are shown. The in-plane magnetization is represented by blue-white-red (black-gray-white) color map.

frequency of the uniform precession mode given by $\omega = \gamma H_{eff}$ and ϕ is the initial phase of oscillation.[22] Here, α_{eff} is the "effective" damping coefficient as opposed to the intrinsic Gilbert damping,[25] γ is the gyromagnetic ratio and H_{eff} is the effective magnetic field which includes the external bias field, demagnetizing field, and anisotropy field.

In Figs. 3(a) and 3(b) we have plotted the precession frequency, the peak amplitude of the out-of-plane component of precession (M_z) and α_{eff}, respectively, as a function of the w/s ratio of the arrays for square elements of 60 nm width and 5 nm thickness at a bias field H_{bias}=500 Oe. The peak value of M_z reduces to about 10% of the single element value in the array with w/s=0.5. With the increase in w/s ratio the peak value of M_z increases and reaches to about 60% of the single element value for w/s=3. The precession frequency of arrays increases almost linearly with the increase in the w/s ratio. The only interaction that changes with the interelement spacing in the arrays is the dipolar interaction. The enhanced interelement dipolar interaction with the increase in w/s ratio suppresses the demagnetizing effect in the individual magnetic elements. Consequently, the effective magnetic field H_{eff}, which is the difference between the bias field and the demagnetizing field, increases and the resulting precession frequency ω also increases with the increase in w/s ratio. For w/s ratio >1 a number of precession modes appear. These are the collective modes of precession in an array,[31,32] which will be described in detail later in this paper. The effective damping coefficient α_{eff} for the single square element is found to be 0.0215 as opposed to the bulk value of 0.008 for permalloy used in the simulation. This enhancement of α_{eff} for the single element is due to the self-dephasing of edge and center modes within the square element which is clear from Fig. 4(a) and was described in detail elsewhere.[13,30] However, in arrays a further increase in α_{eff} occurs, which increases with the increase in w/s ratio. The rate of increase is initially very steep up to w/s=1 and then slows down and attains a value of 0.03 for w/s=3.

In Figs. 3(c) and 3(d) the precession frequency, the peak value of M_z and α_{eff} are plotted as a function of the w/s ratio for arrays of circular elements with 60 nm width and 5 nm thickness. The peak value of M_z for the single element and arrays follow the same trend as in the case of square elements but there is an overall reduction of about 40% in the circular elements compared to the square elements. The precession frequency of a single circular element is 5.4 GHz as opposed to 4.1 GHz for a single square element of the same width and thickness and at the same bias field. The precession frequency for bulk permalloy at the same bias field (H_{bias}=500 Oe) is 6.65 GHz. The reduction in the precession frequency for the individual square and circular elements is due to the increased volume of the demagnetized region and consequent reduction in the total effective field H_{eff} in those confined structures. The increased demagnetizing field increases the region over which the edge mode appears which is larger for square elements. The effective damping α_{eff} for the square and circular magnetic elements is also affected by the dephasing of the edge and the center modes. Due to the larger region over which the edge mode exists, α_{eff} is larger (0.0215) in the individual square element compared to that for the individual circular element (0.017).

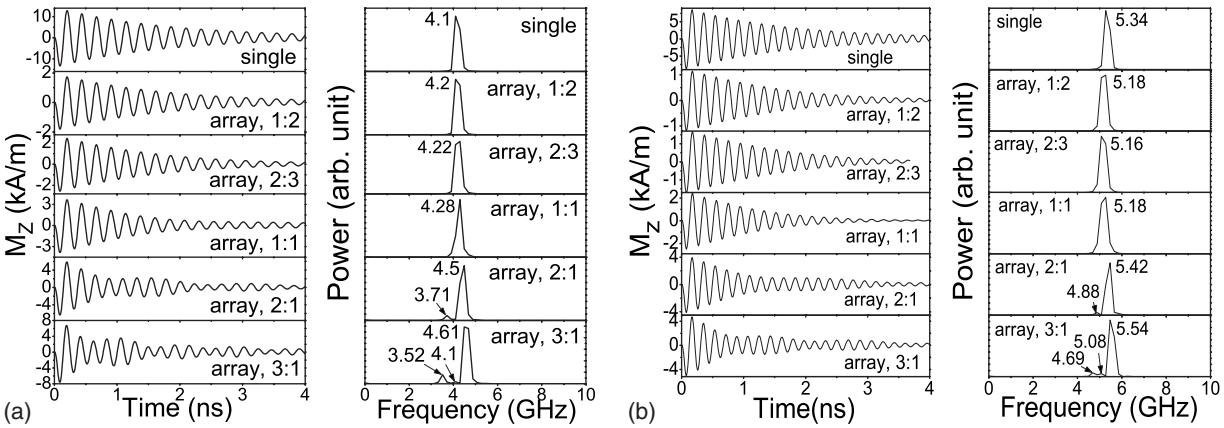

FIG. 2. Time-resolved magnetization (M_Z) and corresponding FFT spectra for single $Ni_{81}Fe_{19}$ elements and arrays of $Ni_{81}Fe_{19}$ elements of (a) square shape and (b) circular shape are shown. The width to separation ratio for the arrays is shown while the peaks in the FFT spectra correspond to the precessional frequencies. A bias field $H_{bias}=500$ Oe is applied in the geometry as shown in Figs. 1(a) and 1(b) for the above simulations. The dimension of the individual element is width=60 nm and thickness=5 nm.

For arrays of circular elements α_{eff} also increases with the w/s ratio and reaches a value of 0.027 for $w/s=1$. Beyond that α_{eff} decreases slightly and nearly saturates at around 0.025.

In order to investigate the origin of increase in α_{eff} in arrays we have analyzed the static and time-resolved images of magnetization for single elements and arrays. Figure 4 shows the time-resolved images from arrays of square elements of varying w/s ratio at two different times corresponding to the first antinode of the precession (~100 ps) and at another antinode that occurs at a much later time scale (>1 ns). For comparison, we show the static and time-resolved magnetic images at the first two antinodes of the single square element in Fig. 4(a) that reveals the edge and center modes of precession. In the arrays [Figs. 4(b)–4(f)] the precessional modes are significantly modified to the extent determined by the spacing between the elements. For arrays of square elements with w/s ratio up to 1, the dynamics at the first antinode is nearly uniform, however at a later time scale (>1 ns) the collective dynamics of the array becomes increasingly incoherent with different elements in the array precessing at different phases. For $w/s=0.5$ and 0.75 only few elements near the edges of the arrays precess out of phase to the other elements. However, for $w/s=1$ a large number of elements precess out of phase to the neighboring elements in the array. This results in a net higher cancellation of the precession amplitude and consequently a very high value of α_{eff}. For $w/s>1$, the precession of different elements in the arrays is incoherent even at the first antinode, revealing complicated mode structure within individual elements, which continues to increase at a later time scale. Hence, for these arrays, in addition to a further increase in α_{eff} we also observe a number of collective precession modes that are distinctly different from the precession modes within a single element.

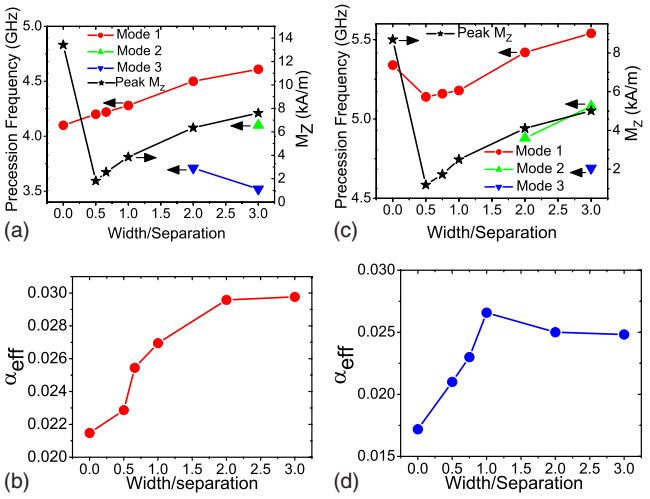

FIG. 3. (Color online) (a) The peak amplitude of precession (M_z) and precession frequencies of a single $Ni_{81}Fe_{19}$ element and arrays of $Ni_{81}Fe_{19}$ elements of square shape are plotted as a function of width to separation ratio. (b) The variation in effective damping (α_{eff}) of magnetization precession with the width to separation ratio in arrays of square $Ni_{81}Fe_{19}$ elements is shown. (c) The peak amplitude of precession (M_z) and precession frequencies of a single $Ni_{81}Fe_{19}$ element and arrays of $Ni_{81}Fe_{19}$ elements of circular shape are plotted as a function of width to separation ratio. (d) The variation in effective damping (α_{eff}) of magnetization precession with the width to separation ratio in arrays of circular $Ni_{81}Fe_{19}$ elements is shown. The dimension of the individual element is width=60 nm and thickness=5 nm.

For arrays of circular elements (Fig. 5) the out-of-phase precession is localized within the elements in the fifth row for $w/s=0.5$ and at the edges of the array for $w/s=0.75$. For $w/s=1$, nearly every element in the array precesses out of phase to its neighboring elements at 1260 ps. The out-of-phase precessions of the elements next to each other cancel the overall precession of the array resulting in the highest value of $\alpha_{eff}=0.027$ for arrays of circular elements. However for $w/s>1$ a different scenario is observed. The elements near the center of the array precess out of phase to the elements near the edges resulting in a smaller region of antiparallel configuration of dynamic magnetization. Consequently α_{eff} decreases slightly in these arrays compared to the array with $w/s>1$.

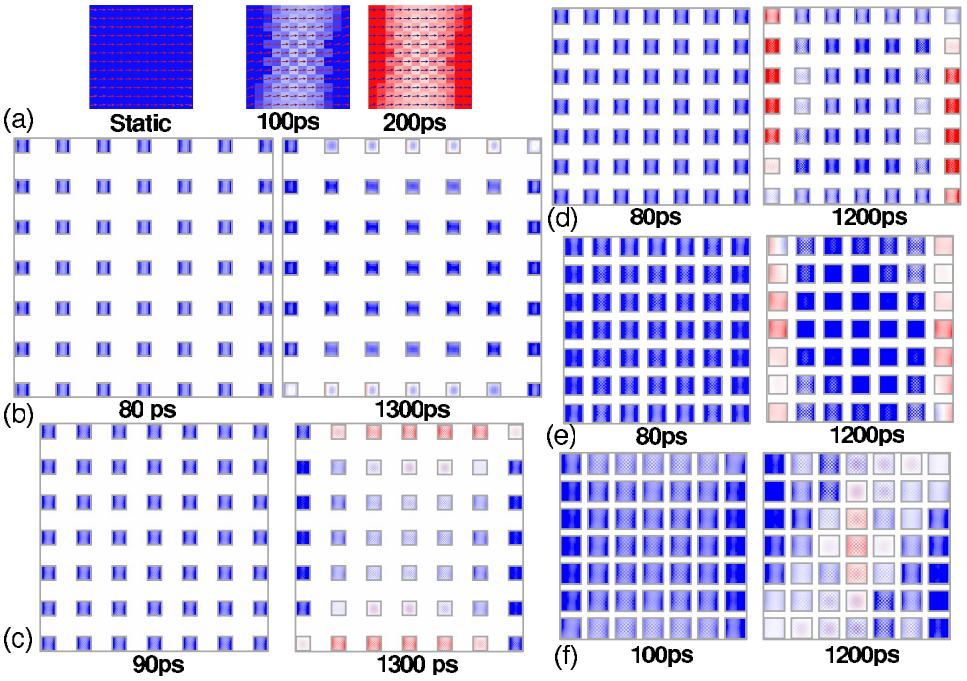

FIG. 4. (Color online) (a) The simulated static magnetic image and the dynamic magnetic images at the first two antinodes (100 and 200 ps) of the time-resolved precession for a single square $Ni_{81}Fe_{19}$ element are shown. The dynamic magnetic images at the first antinode and at another antinode after >1 ns from arrays of square $Ni_{81}Fe_{19}$ elements with width to separation ratio of (b) 1:2, (c) 2:3, (d) 1:1, (e) 2:1, and (f) 3:1 are shown. The dimension of the individual element is width=60 nm and thickness=5 nm. The out-of-plane magnetization is represented by blue-white-red (black-gray-white) color map.

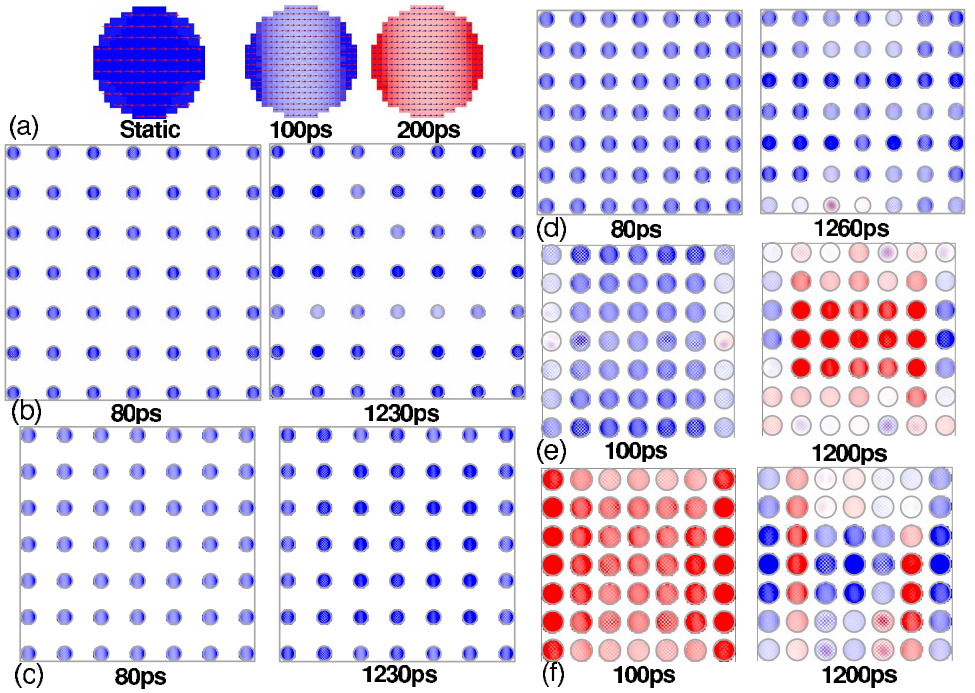

FIG. 5. (Color online) (a) The simulated static magnetic image and the dynamic magnetic images at the first two antinodes (100 and 200 ps) of the time-resolved precession for a single circular $Ni_{81}Fe_{19}$ element are shown. The dynamic magnetic images at the first antinode and at another antinode after >1 ns from arrays of circular $Ni_{81}Fe_{19}$ elements with width to separation ratio of (b) 1:2, (c) 2:3, (d) 1:1, (e) 2:1, and (f) 3:1 are shown. The dimension of the individual element is width=60 nm and thickness=5 nm. The out-of-plane magnetization is represented by blue-white-red (black-gray-white) color map.

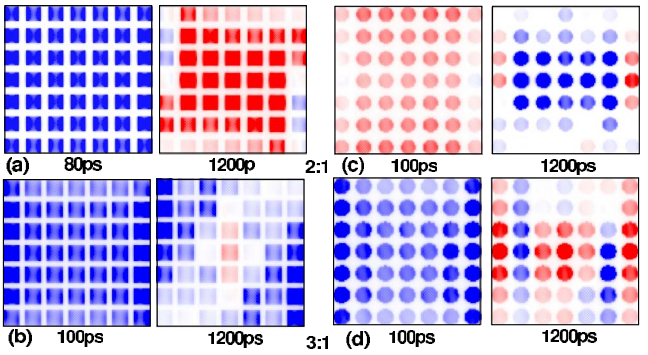

FIG. 6. (Color online) The simulated dipolar magnetic-field images of arrays of square [(a) and (b)] and circular [(c) and (d)] $Ni_{81}Fe_{19}$ elements are shown at two different times. The width to separation ratio of the array is 2:1 for (a) and (c) and 3:1 for (b) and (d). The dimension of the individual element is width=60 nm and thickness=5 nm. The out-of-plane magnetization is represented by blue-white-red (black-gray-white) color map.

To understand the origin of the collective precessional modes in arrays of square and circular elements we have calculated the dipolar field and the total magnetic field acting on every element in the arrays. Since the total magnetic field images provide the same contrasts as the dipolar field images, we presented in Fig. 6 only the dipolar field images in arrays of square and circular elements with w/s ratio=2 and 3 where the effects are most prominent. The dipolar field on individual elements in arrays at the first antinode of precession and at a later time scale (>1 ns) resembles exactly the time-resolved magnetization images showing the origin of the different precessional modes in an array in the dipolar field itself. The precession of different groups of elements in an array at different frequencies causes the splitting of the precessional modes as shown in Fig. 2. Such splitting of modes in arrays are also experimentally observed by various groups.[12,21,31] In order to understand the spatial variation in the individual modes in arrays of elements we have further simulated the response of arrays to sinusoidal fields of frequencies equal to the precessional mode frequencies. Each resonant mode may be individually excited by replacing the pulsed field with a sinusoidal field that oscillates at the resonance frequency. In our simulation a sinusoidal field of form

$$h_{ac} = h_{ac0}(1 - e^{-at})\sin 2\pi ft \tag{2}$$

was applied, with the field amplitude h_{ac0} set to a value of 12 Oe. Variation in h_{ac0} between 3 and 50 Oe did not give any appreciable change in the simulation results. The exponent a was chosen so that the sinusoidal field grew to full amplitude within a few cycles of oscillation. A static field of 500 Oe was applied to the sample to set f, the resonance frequency. A slightly higher damping coefficient of 0.05 was chosen so that other modes, which appear immediately after the application of the ac field, dissipate quickly leaving only the mode corresponding to the frequency of the driving field. Figure 7 shows the out-of-plane component of magnetization from arrays of square and circular elements with $w/s=3$ after 50 cycles of oscillation for phase values of $\pi/2$ and $3\pi/2$ during a single cycle of the sinusoidal driving field. For each

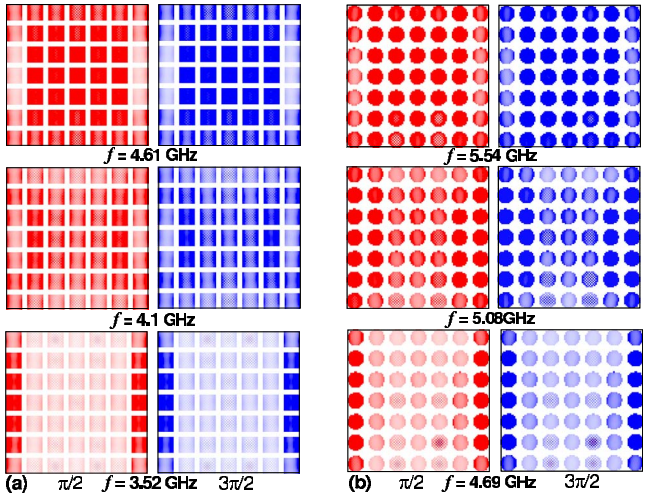

FIG. 7. (Color online) Simulations of the time evolution of the magnetization of arrays of (a) square and (b) circular $Ni_{81}Fe_{19}$ elements with $w/s=3:1$ at different phases during one cycle of the sinusoidal field are shown. The static field (H=500 Oe) and the sinusoidal field (h_{ac0}=12 Oe) with various resonance frequencies f were applied in the geometry as shown in Figs. 1(a) and 1(b). The out-of-plane magnetization is represented by blue-white-red (black-gray-white) color map.

simulation f is set at the resonance mode frequencies. The highest frequency mode (4.61 GHz for the square element and 5.54 GHz for the circular element) has significant amplitude over the entire array apart from the demagnetized regions close to the edges. The intermediate frequency mode (4.1 GHz for the square element and 5.08 GHz for the circular element) is localized in a region halfway between the edge and the center of the array. The lowest frequency mode (3.52 GHz for the square element and 4.69 GHz for the circular element) is localized only in the elements at the edges perpendicular to the bias magnetic field. The observed spatial variations of the time-resolved magnetization in response to a pulsed field in the arrays are a result of the superposition of the three resonant modes as discussed above. The images show that the spatial variation in magnetization in response to the sinusoidal field is identical for arrays of square and circular elements. Moreover, the spatial variation in the collective modes in arrays of square and circular elements are similar to the self-magnetostatic modes observed in single square microscale elements.[29,30] These indicate that in closely packed arrays the collective precession modes are dominated by the size and shape of the array itself and not by that of the individual elements.

We have performed further simulations on arrays of elements with width×thickness=150 nm×50 nm and 150 nm×10 nm. In these elements we clearly observe quasiuniform static magnetization states at a bias field of H_{bias} =500 Oe as shown in Fig. 8(a). The 150 nm×50 nm square element shows an "S" state while the 150 nm ×10 nm square element shows a "C" state. Figure 8(b) shows the static magnetization for the circular elements. The 150 nm×50 nm circular element shows a vortex state with its core shifted perpendicular to the direction of the bias field while the 150 nm×10 nm circular element shows a single

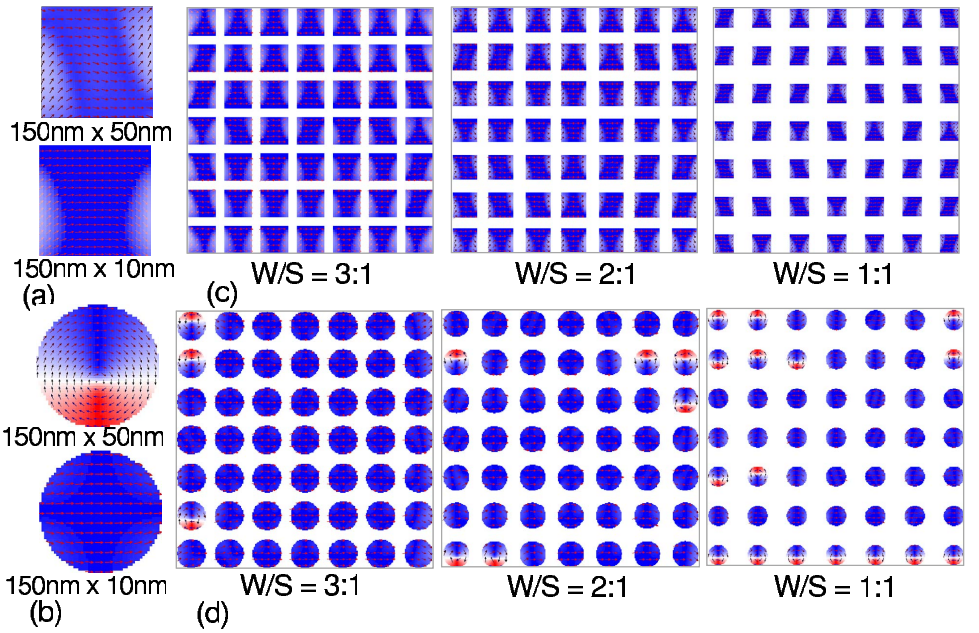

FIG. 8. (Color online) The simulated static magnetic images for (a) square and (b) circular magnetic elements of width × thickness = 150 nm × 50 nm and 150 nm × 10 nm are shown. The static magnetic images of arrays of (c) square and (d) circular magnetic elements of width to separation ratios of 3:1, 2:1, and 1:1 are shown. The dimension of individual elements in the arrays is width = 150 nm and thickness = 50 nm. The in-plane magnetization is represented by blue-white-red (black-gray-white) color map.

domain state. When assembled in arrays various elements take various magnetization configurations. The arrays of square elements (150 nm × 50 nm) have a distribution of "S," "C" and "uniform" magnetization states [Fig. 8(c)], whose strength and localization vary with the w/s ratio. The circular elements (150 nm × 50 nm) in arrays also take different ground-state magnetic configurations such as single vortex with shifted core with different core polarity ($p = \pm 1$), "C" state and uniform magnetization state as shown in Fig. 8(d).

Due to the quasiuniform and nonuniform static magnetizations for the larger elements (150 nm width with varying thickness) the precessional dynamics of the single elements are intrinsically nonuniform showing a number of modes. The time-resolved magnetization dynamics from the single square element and arrays of square elements of 150 nm width and 50 nm thickness are shown in Fig. 9(a). The single square element clearly shows two precessional modes at 1.55 and 4.75 GHz. In arrays both modes have been shifted to higher frequencies. The lower frequency mode is split into three modes while the higher frequency mode is split into two modes. Consequently the dynamic magnetization gets dephased very quickly due to the superposition of all these modes and after a few prominent oscillations a low amplitude complicated oscillatory behavior is observed. It is not appropriate to quantify the dynamics by a single damping coefficient but qualitatively the damping increases with w/s ratio in these arrays.

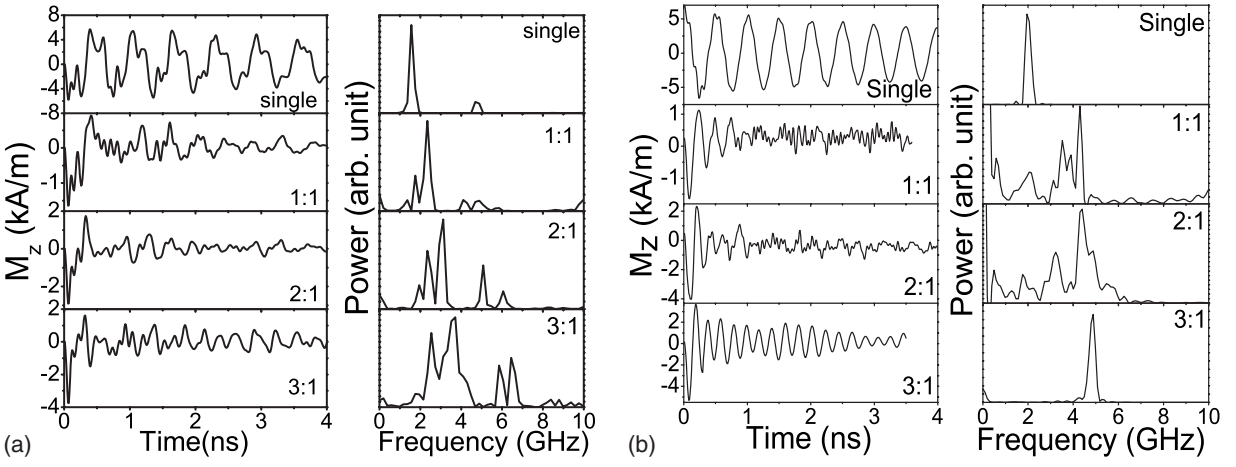

FIG. 9. Time-resolved magnetization (M_z) and corresponding FFT spectra for single elements and arrays of $Ni_{81}Fe_{19}$ elements where the individual elements are (a) square and (b) circular. The dimension of the individual element is width = 150 nm and thickness = 50 nm.

For circular elements the situation is entirely different as the single element and arrays of elements take different magnetic ground states as shown in Figs. 8(b) and 8(d). As a result magnetization dynamics at two different time scales are observed in the single element and arrays as shown in Fig. 9(b). The vortex core oscillation in the single element is long lasting and shows negligible damping within the investigated time scale. The higher frequency precession signal is superposed on the slow vortex core oscillation and shows a sign of decay. When assembled in arrays the strong interelement interaction breaks the vortex state and introduces a single or quasi-single domain configuration for majority of the elements near the center of the arrays. A number of elements near the edges still take a single vortex state with shifted core due to the lack of the symmetry of the dipolar field. With increasing w/s ratio the strength of the dipolar field and hence the magnetic ordering of the elements near the center of the arrays increases. For the array with $w/s=1$, a few shifted core vortex states appear near the center of the array, but they disappear from the center of the array for arrays with $w/s>1$, and the total number of elements in a vortex state decreases as the w/s ratio increases. As a result the dynamics which is a pure vortex core oscillation for the single element is dominated by spin-wave precession in arrays. For arrays with w/s ratio$=1$ and 2, the static magnetic states of the elements in the array are different from each other [Fig. 8(d)]. Consequently, the number of spin-wave modes is large due to the incoherent precession of different elements. With the increase in w/s ratio the coherence in the static magnetic configuration increases[33] and for $w/s=3$ a dominant single mode precession is observed. Unlike for the arrays of square elements, for arrays of circular elements the increased packing density of the array increases the coherence of precession and reduces the effective damping. Nevertheless the dynamics of the arrays of elements is still modified from the intrinsic dynamics of single nanomagnets.

IV. CONCLUSIONS

Dipolar interaction between elements in arrays affects the magnetic ground state and the dynamics in different ways. The static magnetic configuration is modified and in some cases is changed into a different domain state in arrays depending on the symmetry and strength of the interelement interaction, which is quantified by the w/s ratio in this paper. In arrays of square and circular elements where the static magnetic configuration for the single element is uniform or quasiuniform the effect of interelement interaction introduces only minor changes in the magnetization. For example, in the arrays of square and circular elements of 60 nm width and 5 nm thickness only small demagnetized regions near the edges of the elements are observed even in densely packed arrays. On the other hand for arrays of square elements of 150 nm width and 50 nm thickness a distribution of various static magnetization states such as "C," "S," and uniformly magnetized states are observed. The symmetry of the element itself and that of the dipolar field play significant roles to decide the static magnetization in arrays. For the 150 nm$\times$50 nm circular elements the symmetry forces the single element to take a vortex state with shifted core at $H_{\mathrm{bias}}=500$ Oe. However, the strength and symmetry of the dipolar interaction in square arrays destroy the vortex state in majority of the individual elements and a distribution of single vortex state of different core polarization, "C," "S," and quasiuniform magnetization states are observed.

The dynamics in arrays is affected in many different ways. The precession frequency shows a general trend to increase with the increase in the width/separation ratio. Splitting of a single precession mode into a number of modes for sufficiently high w/s ratio is also observed. For circular elements (150 nm$\times$50 nm) the array effect changes the mechanism of the dynamics from a slow vortex core oscillation to incoherent and nearly coherent spin-wave dynamics. The peak amplitude of precession is significantly reduced in sparsely packed arrays. While the peak amplitude of precession increases with increase in packing density, it still remains significantly lower compared to the single element. However, the most fascinating effect of the interelement interaction in arrays is the modification of the effective damping coefficient α_{eff}. Analysis of dynamic magnetic images clearly shows that the increase in α_{eff} is a result of increased dephasing of precession of various elements in an array. With the increase in the w/s ratio the amount of out-of-phase precession between neighboring elements increases which results in a drastic net cancellation of the amplitude of precession that manifests as an increased effective damping. For arrays of larger elements where the intrinsic dynamics of the single nanomagnet itself is incoherent the array effect only increases the incoherence and introduces more precessional modes and increases the overall damping. We have shown that the dipolar field on the elements in an array governs their static and dynamic magnetization behaviors. In addition, the collective modes of the elements in an array are determined by the shape and size of the array itself. We conclude that the ordered arrays of magnetic nanoelements show static and dynamic magnetic properties which are different in many ways from the intrinsic dynamics of single nanomagnet as discussed above.

ACKNOWLEDGMENTS

The authors thank Holger Schmidt for useful discussions. One of the authors (S.B.) acknowledges the financial assistance (Grant No. SR/FTP/PS-71/2007) of the Department of Science and Technology, Government of India.

*abarman@physics.iitd.ac.in

[1] B. D. Terris and T. Thomson, J. Phys. D **38**, R199 (2005).
[2] I. N. Krivorotov, N. C. Emley, J. C. Sankey, S. I. Kiselev, D. C. Ralph, and R. A. Buhrman, Science **307**, 228 (2005).
[3] Y. Togawa, T. Kimura, K. Harada, T. Matsuda, A. Tonomura, Y. Otani, and T. Akashi, Appl. Phys. Lett. **92**, 012505 (2008).
[4] G. Reiss and A. Hütten, Nature Mater. **4**, 725 (2005).
[5] S. H. Chung, A. Hoffmann, S. D. Bader, C. Liu, B. Kay, L. Makowski, and L. Chen, Appl. Phys. Lett. **85**, 2971 (2004).
[6] E. A. Anderson, S. Isaacman, D. S. Peabody, E. Y. Wang, J. W. Canary, and K. Kirshenbaum, Nano Lett. **6**, 1160 (2006).
[7] R. A. McMillan, C. D. Paavola, J. Howard, S. L. Chan, N. J. Zaluzec, and J. D. Trent, Nature Mater. **1**, 247 (2002).
[8] S. D. Bader, Rev. Mod. Phys. **78**, 1 (2006).
[9] O. Hellwig, A. Berger, T. Thompson, E. Dobisz, Z. Z. Bandic, H. Yang, D. S. Kercher, and E. E. Fullerton, Appl. Phys. Lett. **90**, 162516 (2007).
[10] B. D. Terris, M. Albrecht, G. Hu, T. Thomson, and C. T. Rettner, IEEE Trans. Magn. **41**, 2822 (2005).
[11] R. L. Stamps and R. E. Camley, Phys. Rev. B **60**, 12264 (1999).
[12] S. Jung, B. Watkins, L. DeLong, J. B. Ketterson, and V. Chandrasekhar, Phys. Rev. B **66**, 132401 (2002).
[13] V. V. Kruglyak, A. Barman, R. J. Hicken, J. R. Childress, and J. A. Katine, Phys. Rev. B **71**, 220409(R) (2005).
[14] K. S. Buchanan, X. Zhu, A. Meldrum, and M. R. Freeman, Nano Lett. **5**, 383 (2005).
[15] Z. K. Wang, H. S. Lim, V. L. Zhang, J. L. Goh, S. C. Ng, M. H. Kuok, H. L. Su, and S. L. Tang, Nano Lett. **6**, 1083 (2006).
[16] J. M. Florczak and E. D. Dahlberg, J. Appl. Phys. **67**, 7520 (1990).
[17] P. Kabos, A. B. Kos, and T. J. Silva, J. Appl. Phys. **87**, 5980 (2000).
[18] P. K. Wei, H. L. Chou, You-Ren Cheng, and Y. D. Yao, J. Appl. Phys. **98**, 093904 (2005).
[19] W. K. Hiebert, A. Stankiewicz, and M. R. Freeman, Phys. Rev. Lett. **79**, 1134 (1997).
[20] R. P. Cowburn, D. K. Koltsov, A. C. Adeyeye, and M. E. Welland, Appl. Phys. Lett. **73**, 3947 (1998).
[21] A. Barman, S. Wang, J. D. Maas, A. R. Hawkins, S. Kwon, A. Liddle, J. Bokor, and H. Schmidt, Nano Lett. **6**, 2939 (2006).
[22] A. Barman, S. Wang, J. Maas, A. R. Hawkins, S. Kwon, A. Liddle, J. Bokor, and H. Schmidt, Appl. Phys. Lett. **90**, 202504 (2007).
[23] Z. Liu, R. D. Sydora, and M. R. Freeman, Phys. Rev. B **77**, 174410 (2008).
[24] K. Y. Guslienko, V. Novosad, Y. Otani, H. Shima, and K. Fukamichi, Phys. Rev. B **65**, 024414 (2001).
[25] L. D. Landau and E. Lifshitz, Phys. Z. Sowjetunion **8**, 153 (1935); T. L. Gilbert, Phys. Rev. **100**:1243 (1955) [Abstract only; full report, Armor Research Foundation Project No. A059, Supplementary Report, May 1, 1956] (unpublished).
[26] M. Donahue and D. G. Porter, *OOMMF User's Guide*, Version 1.0, Interagency Report NISTIR 6376 (National Institute of Standard and Technology, Gaithersburg, MD, 1999); http://math.nist.gov/oommf
[27] S. Jung, J. B. Ketterson, and V. Chandrasekhar, Phys. Rev. B **66**, 132405 (2002).
[28] M. J. Donahue and D. G. Porter, Physica B **343**, 177 (2004).
[29] A. Barman and R. C. Sharma, J. Appl. Phys. **102**, 053912 (2007).
[30] A. Barman, V. V. Kruglyak, R. J. Hicken, J. M. Rowe, A. Kundrotaite, J. Scott, and M. Rahman, Phys. Rev. B **69**, 174426 (2004).
[31] P. S. Keatley, V. V. Kruglyak, A. Neudert, E. A. Galaktionov, R. J. Hicken, J. R. Childress, and J. A. Katine, Phys. Rev. B **78**, 214412 (2008).
[32] N. I. Polushkin, S. A. Michalski, L. Yue, and R. D. Kirby, Phys. Rev. Lett. **97**, 256401 (2006).
[33] R. P. Cowburn, A. O. Adeyeye, and M. E. Welland, N. J. Phys. **1**, 16 (1999).